

Find Them All: Unveiling MLLMs for Versatile Person Re-identification

Jinhao Li¹, Zijian Chen^{2,4}, Lirong Deng³, Guangtao Zhai^{2,4*}, Changbo Wang^{1*}

¹School of Computer Science and Technology, East China Normal University

²Institute of Image Communication and Information Processing, Shanghai Jiao Tong University,

³Macao Polytechnic University, ⁴Shanghai AI Laboratory

lomljhoax@stu.ecnu.edu.cn, zijian.chen@sjtu.edu.cn, p2523406@mpu.edu.mo,

zhaiguangtao@sjtu.edu.cn, cbwang@cs.ecnu.edu.cn

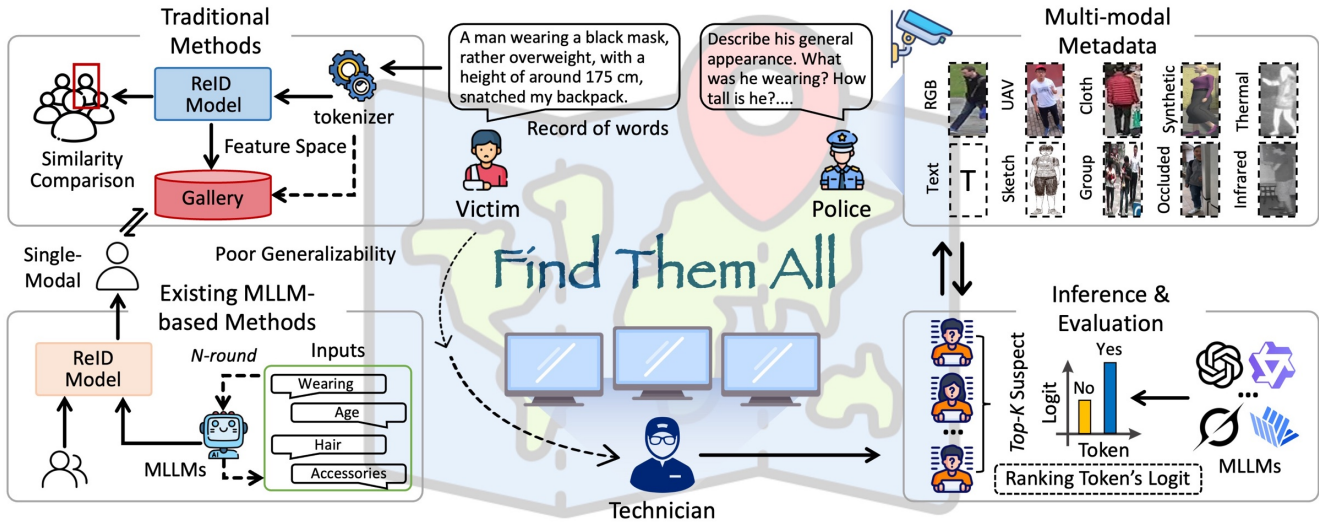


Figure 1. Comparison of different person re-identification (ReID) paradigms. Traditional methods typically matches a query, e.g., a suspect portrait or textual description, against a gallery by comparing high-level features. Similarly, existing MLLM-based methods utilize MLLMs to refine an initial description to gradually align with the target. However, both conventional paradigms predominantly concentrate on a few modalities (e.g., RGB and text), limiting their applicability in diverse real-world scenarios. In this work, we conduct a holistic evaluation for MLLMs on ten different modalities to verify their capabilities in handling person ReID tasks directly.

Abstract

Person re-identification (ReID) aims to retrieve images of a target person from the gallery set, with wide applications in medical rehabilitation and public security. However, traditional person ReID models are typically uni-modal, resulting in limited generalizability across heterogeneous data modalities. Recently, the emergence of multi-modal large language models (MLLMs) has shown a promising avenue for addressing this issue. Despite this potential, existing methods merely regard MLLMs as feature extractors or caption generators, leaving their capabilities in person ReID

tasks largely unexplored. To bridge this gap, we introduce a novel benchmark for *Versatile Person Re-ID*entification, termed *VP-ReID*. The benchmark includes 257,310 multi-modal queries and gallery images, covering ten diverse person ReID tasks. In addition, we propose two task-oriented evaluation schemes for MLLM-based person ReID. Extensive experiments demonstrate the impressive versatility, effectiveness, and interpretability of MLLMs in various person ReID tasks. Nevertheless, they also have limitations in handling a few modalities, particularly thermal and infrared data. We hope that *VP-ReID* can facilitate the community in developing more robust and generalizable cross-

*Corresponding Authors.

1. Introduction

Person re-identification (ReID) aims to retrieve images of an interested person from the gallery images based on multi-modal queries [54]. The input modalities of person ReID vary significantly across different application scenarios, reflecting the diverse requirements of practical deployments. For instance, forensic applications often rely on sketch images drawn by artists and textual descriptions provided by witnesses, while intelligent surveillance systems may utilize thermal or infrared images to identify individuals under low-light conditions. These heterogeneous tasks necessitate the development of diverse input modalities, including RGB, sketch, synthetic, UAV, group, cloth-changing, occluded, thermal, and infrared images [6, 11, 21, 26, 28, 40, 57, 59], as well as textual descriptions [20]. Consequently, the primary challenge lies in designing a unified framework capable of effectively processing and integrating these diverse multi-modal inputs while maintaining robust performance across various real-world scenarios.

As shown in Fig. 1, traditional person ReID methods [18, 55] predominantly focus on developing task-specific models that consist of a specialized tokenizer and retriever. The tokenizer is responsible for feature extraction, while the retriever handles the matching and ranking of candidate gallery images. Furthermore, these specialist components must be precisely paired to ensure optimal performance, meaning that a text tokenizer cannot be effectively paired with a sketch image retriever due to inherent modality disparities. While traditional person ReID approaches have achieved remarkable human-level performance within their respective modalities [5, 58], they exhibit poor generalizability when transferred to other modalities. This fundamental lack of cross-modal generalizability significantly constrains the practical applicability of traditional person ReID methods in real-world scenarios, where diverse and heterogeneous input modalities are commonly encountered.

Recently, multi-modal large language models (MLLMs) have shown impressive performance across various multi-modal tasks [8]. Pioneering works such as Flamingo [1] and LLaVA [29] exemplify the exceptional prowess of MLLMs as powerful visual-language learners. This characteristic holds significant potential for person ReID tasks, particularly in addressing the challenges of cross-modal inputs. Moreover, the inherent interpretability of MLLMs enables a clearer understanding of their decision-making processes. Existing MLLM-based person ReID methods can be categorized into two groups. One group utilizes MLLMs to recognize pedestrian image attributes or extract style features that capture human annotator preferences [20, 44]. The other group leverages MLLMs to generate rich textual

descriptions for each pedestrian image directly [16, 17, 57]. However, these methods still rely on convolutional neural networks (CNN) or Transformer-based retrievers for person ReID, which fail to fully harness the comprehensive reasoning, instruction-following, and cross-modal understanding capabilities of MLLMs, thereby limiting their potential for truly unified multi-modal person ReID systems.

In this paper, we aim to enable MLLMs to directly and precisely retrieve the target individual from a gallery set, regardless of the query modality. To this end, we propose VP-ReID, a novel benchmark for versatile person ReID that encompasses two evaluation schemes: multiple-choice questions (MCQ) and query-gallery matching (QGM). The MCQ performs one-pass multi-choice reasoning, where all gallery images are jointly input for inference, while the QGM adopts a pairwise matching problem that involves multiple rounds of query-gallery inference. Both schemes include ten representative person ReID tasks, each accompanied by a corresponding dataset. In total, our VP-Bench comprises 4,642 query samples and 252,668 gallery images. Furthermore, we adopt a softmax-based evaluation pipeline for the QGM, which transforms the internal logits of output tokens into continuous and comparable matching scores. Finally, we conduct extensive evaluations of two traditional person ReID models, six proprietary MLLMs, and nine open-source MLLMs on our VP-ReID. The results provide an in-depth understanding of the strengths and weaknesses of MLLMs in person ReID tasks, establishing a comprehensive and unified foundation for future research. In conclusion, the contributions of this paper can be summarized as follows:

- We construct VP-ReID, a novel benchmark for evaluating the person ReID capabilities of MLLMs, which contains 4,642 query samples and 252,668 gallery images across ten diverse person ReID tasks.
- We design two evaluation schemes for MLLM-based person ReID: multiple-choice questions (MCQ) and query-gallery matching (QGM), which systematically evaluate their strengths and weaknesses across various modality inputs and reasoning settings.
- We perform comprehensive evaluations of two traditional models, six proprietary MLLMs, and nine open-source MLLMs, offering an in-depth understanding of how MLLMs perform in person ReID tasks.

2. Related Work

2.1. Person Re-identification

Given a query image, the goal of person re-identification (ReID) is to retrieve the target image from a gallery set. Under the mainstream trend of deep learning, CNN-based person ReID methods are typically divided into two categories: closed-world and open-world [54]. The closed-

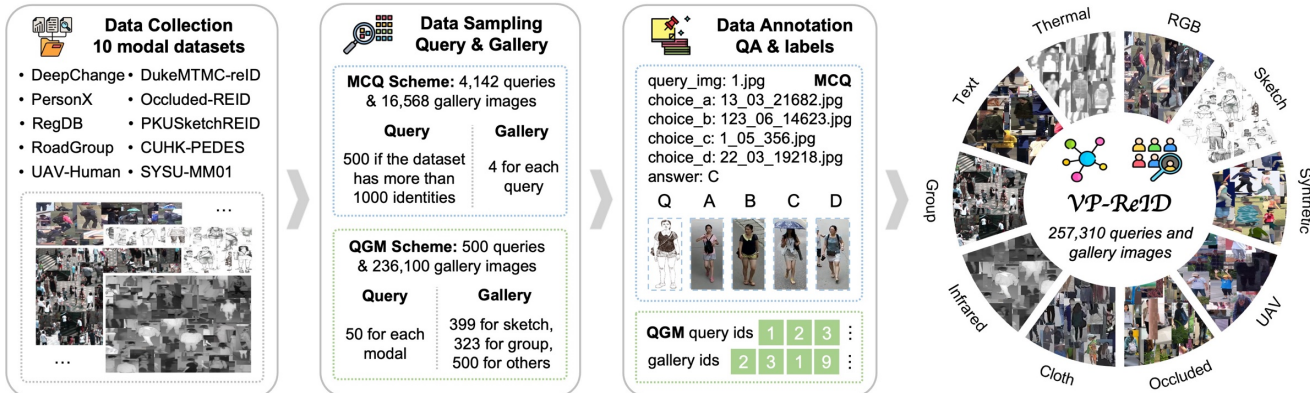


Figure 2. Construction pipeline of the **VP-ReID**. We first collect source contents from ten person ReID datasets covering diverse modalities. Then, queries and gallery images are sampled based on the two proposed evaluation schemes: MCQ and QGM, resulting in a total of 257,310 queries and gallery images. Finally, we organize the data into question–answer pairs for the MCQ and extract labels for the QGM.

world setting focuses on learning discriminative feature representations from well-labeled visible images captured by common video surveillance [56]. In contrast, open-world ReID addresses more complex and challenging scenarios, such as cross-modal ReID [9, 53], unsupervised learning [4, 12], and domain generalization [22, 31]. With the advent of the vision Transformer (ViT) [14], a surge of ViT-based approaches has been proposed for person ReID, achieving remarkable performance on both regular image [25, 62] and cross-modal [37, 41] ReID tasks. Moreover, ViT-based models have demonstrated clear superiority over CNN-based models in video person ReID [47, 48]. However, in the emerging era of MLLMs, the performance of MLLMs in person ReID remains unclear.

2.2. MLLMs in Person Re-identification

Recently, many works have utilized multi-modal large language models (MLLMs) for person ReID. For example, MP-ReID [57] regards ChatGPT as a multi-prompt generator, which contributes to a comprehensive understanding of the input image. Similarly, Instruct-ReID [16] leverages MLLMs to generate instructions encompassing six traditional person ReID tasks. Though MLLMs reduce human labor and annotation time, the generated annotations lack diversity in description styles. To address this issue, TVI-LFM [17] employs an off-the-shelf large language model to augment the generated textual descriptions from the vision language model (VLM), followed by an additional VLM that creates fusion features semantically consistent with visible features. Moreover, IDEA [44] incorporates MLLMs to extract eight predefined attributes from the generated captions and populates these attributes into the same template for more diverse descriptions. Most recently, HAM [20] performs clustering and prompt learning on the extracted textual descriptions, thereby enriching the diversity of the

MLLM-generated captions. Nevertheless, these approaches primarily treat MLLMs as feature extractors or caption generators, failing to fully exploit their capabilities in person ReID tasks.

3. The Proposed VP-ReID

3.1. Scheme Design

To comprehensively evaluate the multi-modal reasoning and retrieval capabilities of MLLMs in person ReID, we propose VP-ReID, a versatile person ReID benchmark that introduces two evaluation schemes: multi-choice questions (MCQ) and query-gallery matching (QGM). In the MCQ, all gallery images are fed into the model simultaneously for inference, enabling direct multi-choice reasoning within a single pass. The model is required to select the correct gallery image from the candidates given a query and a prompt, following a question-answer format. The prediction is considered correct only if the model selects the target gallery image, and the final performance is reported in terms of accuracy. In contrast, the QGM formulates person ReID as a binary matching problem between a query and a gallery image under prompt guidance, where the model outputs a single-word response (Yes or No) to indicate identity consistency. For each query, the model performs multiple rounds of inference, each comparing the query with one gallery image at a time. The evaluation of QGM follows the softmax-based evaluation pipeline described in Sec. 3.3. Besides, both schemes contain ten different person ReID tasks, each accompanied by a corresponding dataset. This design allows the benchmark to systematically analyze the strengths and weaknesses of MLLMs in handling diverse modality inputs and reasoning settings.

Table 1. Statistics of the used datasets and our VP-ReID. For CUHK-PEDES, RegDB, and SYSU-MM01, we report image/text, RGB/thermal, and RGB/infrared in the ‘# Images’ column, respectively. The ‘# Query’ and ‘# Gallery’ of the MCQ and QGM schemes are delimited by slashes.

Datasets	# Images	# Identity	# Query	# Gallery	Type
DukeMTMC-ReID [61]	36,441	1,812	702/50	4/500	RGB
PKUSketchReID [34]	400	200	200/50	4/399	Sketch
PersonX [39]	45,576	1,266	856/50	4/500	Synthetic
UAV-Human [24]	41,290	1,144	119/50	4/500	UAV
Occluded-REID [64]	2,000	200	200/50	4/500	Occluded
DeepChange [51]	178,000	1,121	500/50	4/500	Cloth-changing
RoadGroup [27]	324	162	162/50	4/324	Group
CUHK-PEDES [23]	40,206/80,422	13,003	500/50	4/500	Text
RegDB [30]	4,120/4,120	412	412/50	4/500	Thermal
SYSU-MM01 [45]	20,284/9,929	491	491/50	4/500	Infrared

3.2. Construction Pipeline

Data Collection. As shown in Fig. 2, the VP-ReID benchmark is established by identifying ten representative person ReID tasks, including RGB, sketch, synthetic, UAV, occluded, cloth-changing, group, text, thermal, and infrared person ReID. These tasks are selected for their strong relevance to real-world scenarios and their ability to expose the multi-modal limitations of existing models. Based on the defined tasks, we first investigate the research in these fields and adopt ten commonly used datasets for our experiments. The detailed statistics of these datasets and our VP-Bench are reported in Tab. 1.

Data Sampling. After data collection, we build the MCQ by sampling one query for each identity in these datasets. For datasets containing more than 1,000 identities, we select only 500 queries. The corresponding gallery set for each query is then composed of one positive image from the same identity and three negative images from the remaining identities. For datasets captured by multiple cameras, gallery samples are drawn from different cameras to enhance cross-view diversity. This process yields a total of 4,142 query images and 16,568 gallery images.

For the QGM, we begin by selecting 50 distinct identities from each dataset to form the query set. The gallery set is subsequently assembled by pairing each query with one positive image from the same identity and 499 images from other identities (398 for sketch person ReID and 323 for group person ReID). Similar to the MCQ setting, gallery images are chosen from different cameras. Overall, the VP-ReID benchmark comprises 500 query samples and 236,100 gallery images for the QGM.

Data Annotation. Finally, we annotate the sampled data according to different evaluation schemes. In the MCQ, each instance is represented as a question-answer pair, primarily consisting of three components: (1) the path to the query image or query text, (2) the paths to the gallery images, and (3) an answer grounded in the data collection stage. The gallery images are shuffled to ensure randomness. For each gallery image, we assign a distinct capital letter so that we can prompt the MLLMs to respond solely

with the corresponding letter, thereby facilitating straightforward accuracy computation. In the QGM, we extract the labels of the query samples and gallery images for the evaluation process. In both schemes, each query is paired with only one gallery image that shares the same identity.

3.3. Evaluation Pipeline

To establish a comparative bridge between traditional models and MLLMs in person ReID tasks, we adopt a softmax-based evaluation strategy [46] to transform the output tokens of MLLMs into continuous and comparable matching scores. For each gallery image g_j in the QGM, the MLLMs are required to provide a single-word response $x_j \in \{\text{Yes}, \text{No}\}$ reflecting their decision on identity consistency. By applying a softmax operation over the internal logits corresponding to the tokens $\text{Yes}(x_j^{\text{Yes}})$ and $\text{No}(x_j^{\text{No}})$, the matching confidence for the query-gallery pair is computed as:

$$p_j = \frac{e^{x_j^{\text{Yes}}}}{e^{x_j^{\text{Yes}}} + e^{x_j^{\text{No}}}}. \quad (1)$$

For a given query q_i , with a gallery set size of G , we obtain a distance vector:

$$s_i = [1 - p_1^i, 1 - p_2^i, \dots, 1 - p_G^i]. \quad (2)$$

By ranking the gallery images in ascending order of the scores in s_i , we can derive the traditional person ReID metrics, such as CMC and mAP:

$$\text{CMC}(k) = \frac{1}{Q} \sum_{i=1}^Q \mathbf{1}[\min_{g_j \in \mathcal{P}_i} \text{rank}(g_j) \leq k], \quad (3)$$

$$\text{mAP} = \frac{1}{Q} \sum_{i=1}^Q \text{AP}_i. \quad (4)$$

where Q is the number of queries, \mathcal{P}_i is the set of correctly matched gallery images for query q_i , and AP_i refers to the average precision for query q_i .

4. Experiments

4.1. Experimental Setup

Our experiments evaluate a total of 15 MLLMs, encompassing a diverse mix of proprietary and open-source models. For proprietary models, we adopt OpenAI models (GPT-4o [32] and GPT-4.1 [33]), Google’s Gemini models (Gemini 2.0 Flash [36] and Gemini 1.5 Pro [42]), and Grok models (Grok-2 [49] and Grok-4 [50]). For open-source models, we cover the Qwen2.5-VL [2], Qwen3-VL [52], and InternVL families, including InternVL2.5 [7], InternVL3 [63], and InternVL3.5 [43]. To enable a more comprehensive comparison, we also include representative traditional models. Specifically, we adopt TransReID [15], a transformer-based

Table 2. Performance (*Accuracy*) comparisons of evaluated MLLMs on ten person ReID tasks under the MCQ setting. We use the *instruct* version for all open-source MLLMs. The best and second-best results are in **bold** and underlined, respectively.

Model	Cloth	RGB	Occluded	Synthetic	Sketch	Thermal	Text	Group	Infrared	UAV	Avg.
Proprietary MLLMs:											
Grok-2 [49]	0.27	0.26	0.33	0.29	0.46	0.25	0.25	0.21	0.25	0.29	0.29
Grok-4 [50]	0.29	0.25	0.17	0.30	0.66	0.29	0.23	0.21	0.35	0.24	0.30
Gemini-1.5-Pro [42]	0.68	0.84	<u>0.98</u>	<u>0.99</u>	0.92	0.33	<u>0.97</u>	0.98	0.51	0.76	0.80
Gemini-2.0-Flash [36]	0.67	0.85	0.96	0.98	0.97	<u>0.46</u>	<u>0.95</u>	0.98	0.53	<u>0.83</u>	0.82
GPT-4o [32]	0.71	0.86	0.97	<u>0.99</u>	0.95	0.39	<u>0.97</u>	0.94	0.49	0.63	0.79
GPT-4.1 [33]	0.79	0.92	0.99	1.00	<u>0.96</u>	0.60	0.98	<u>0.96</u>	0.63	0.76	0.86
Open-Source MLLMs:											
Qwen2.5-VL-3B [2]	0.27	0.25	0.26	0.30	0.30	0.28	0.22	0.32	0.23	0.32	0.28
Qwen2.5-VL-7B [2]	0.49	0.66	0.67	0.95	0.80	0.34	0.75	0.83	0.46	0.63	0.69
Qwen2.5-VL-32B [2]	0.57	0.76	0.85	0.98	0.83	0.36	0.81	0.86	0.52	0.82	0.75
Qwen3-VL-2B [52]	0.56	0.62	0.76	0.85	0.77	0.35	0.68	0.72	0.45	0.63	0.66
Qwen3-VL-4B [52]	0.71	0.83	0.89	<u>0.99</u>	0.90	0.39	0.90	<u>0.96</u>	0.53	0.71	0.82
Qwen3-VL-8B [52]	0.71	0.88	0.97	<u>0.99</u>	0.88	<u>0.46</u>	0.90	<u>0.96</u>	<u>0.59</u>	0.85	<u>0.84</u>
Qwen3-VL-32B [52]	0.68	<u>0.89</u>	0.96	0.98	0.84	0.40	0.91	0.98	0.56	0.82	0.83
InternVL3.5-8B [43]	0.61	0.65	0.96	0.95	0.74	0.30	0.26	0.84	0.39	0.65	0.66
InternVL3.5-38B [43]	<u>0.75</u>	0.75	0.85	1.00	0.88	0.36	0.25	0.98	0.58	0.81	0.72

Table 3. Performance (*mAP*) comparisons between traditional models and MLLMs on ten person ReID tasks under the QGM setting. For the ‘Text’ column, we use IRRA [19] as the traditional baseline and obtain an mAP of 0.59. We use the *instruct* version for all evaluated MLLMs. The best and second-best results are in **bold** and underlined, respectively.

Model	Cloth	RGB	Occluded	Synthetic	Sketch	Thermal	Text	Group	Infrared	UAV	Avg.
Traditional Models:											
TransReID [15]	0.52	0.73	0.77	<u>0.95</u>	0.16	0.02	–	0.56	0.03	0.60	0.48
Open-Source MLLMs:											
Qwen2.5-VL-3B [2]	0.03	0.06	0.11	0.43	0.22	0.02	0.45	0.12	0.07	0.21	0.20
Qwen2.5-VL-7B [2]	0.25	0.47	0.37	0.60	0.39	<u>0.08</u>	0.55	0.56	0.11	0.33	0.44
Qwen2.5-VL-32B [2]	0.22	0.45	0.23	0.77	0.37	0.03	0.55	0.57	0.06	0.31	0.43
Qwen3-VL-2B [52]	0.33	0.43	0.46	0.87	0.48	0.09	0.58	0.65	0.07	0.37	0.52
Qwen3-VL-4B [52]	<u>0.49</u>	<u>0.66</u>	<u>0.74</u>	0.99	0.60	0.04	<u>0.74</u>	0.80	0.14	0.43	<u>0.68</u>
Qwen3-VL-8B [52]	<u>0.49</u>	0.57	0.63	<u>0.95</u>	<u>0.77</u>	0.09	0.68	<u>0.84</u>	0.17	<u>0.54</u>	<u>0.68</u>
Qwen3-VL-32B [52]	0.46	0.57	0.63	0.89	0.78	0.09	0.83	0.92	<u>0.16</u>	0.43	0.69
InternVL3.5-8B [43]	0.22	0.04	0.66	0.28	0.10	0.02	0.01	0.05	0.02	0.04	0.18
InternVL3.5-38B [43]	0.31	0.47	0.66	0.98	0.32	0.03	0.00	0.15	0.06	0.22	0.39

object ReID framework that achieves strong performance across various benchmarks. For the text person ReID, we employ IRRA [19], a cross-modal ReID framework that models the relationships between local visual and textual tokens while enhancing global image-text matching without relying on additional prior supervision. All traditional models are reproduced using their publicly available code.

4.2. Main Results

Results on the MCQ. As shown in Tab. 2, proprietary MLLMs outperform open-source counterparts, with GPT-4.1 achieving the highest average accuracy of 0.86. Notably, GPT-4.1 attains 0.60 and 0.63 on the thermal and infrared person ReID tasks, exceeding the second-best results by

0.14. Meanwhile, open-source MLLMs also demonstrate competitive performance. For example, Qwen3-VL-8B and Qwen3-VL-32B achieve the best results on UAV and group person ReID tasks, respectively. These results offer an initial overview of the MLLMs’ performance on person ReID tasks. To enable a comprehensive comparison between traditional models and MLLMs, we focus on the QGM evaluation scheme for further analysis and discussion in the following experiments.

Results on the QGM. The performance of MLLMs on the QGM is reported in Tab. 3 and Fig. 3. On the one hand, several MLLMs (e.g., Qwen3-VL family) obtain remarkable results on tasks such as RGB, occluded, synthetic, sketch, text, and group person ReID. Notably, Qwen3-VL-

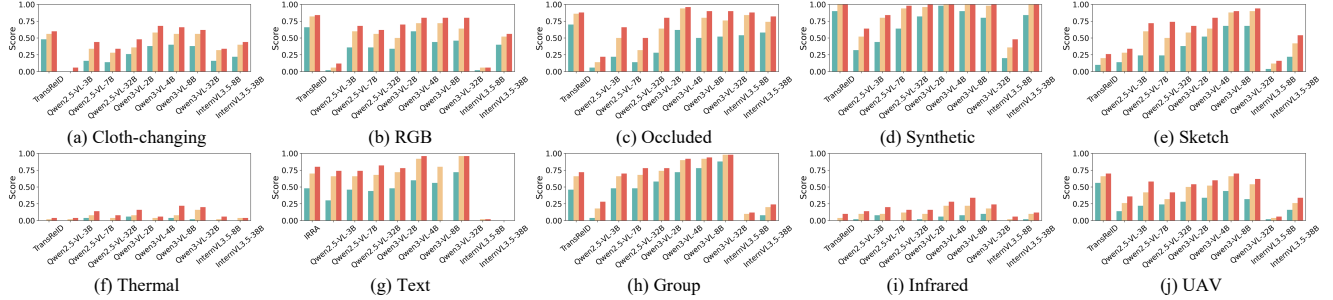


Figure 3. Performance (CMC) comparisons between traditional models and MLLMs on ten person ReID tasks under the QGM setting.

32B achieves an impressive mAP of 0.83 on the text person ReID task and 0.92 on the group person ReID task, effectively retrieving nearly all target images without any training data. On the other hand, MLLMs also show substantial limitations in VP-ReID. For example, they struggle significantly with thermal and infrared person ReID tasks. Quantitatively, even the best-performing model attains only 0.09 and 0.17 in mAP on thermal and infrared tasks, respectively. This degradation in performance may stem from the inherent information loss in these modalities, as well as from the absence of domain-specific training data for MLLMs.

Comparisons with Traditional Person ReID Models. To ensure a more comprehensive comparison, we adopt two traditional person ReID models, TransReID and IRRA, which were trained on Market-1501 [60] and ICFG-PEDES [13], respectively. In contrast, the MLLMs are evaluated in a zero-shot setting. We present the results in Tab. 3 and Fig. 3. It can be observed that TransReID achieves state-of-the-art results on cloth-changing, RGB, occluded, and UAV person ReID tasks. However, the performance gap between the MLLMs and TransReID is relatively small. In particular, the difference in mAP is less than 0.03 in the cloth-changing and occluded person ReID tasks. Moreover, the MLLMs outperform TransReID by a large margin in sketch and group person ReID tasks, highlighting their superior cross-modal capabilities. Similarly, Qwen3-VL-32B surpasses IRRA by 0.24 in Rank@1 and mAP on the text person ReID task. These results indicate that, while traditional models perform well on specific modalities, MLLMs can achieve comparable performance in these modalities and significantly outperform them in others.

MLLMs Perform Poorly on Thermal and Infrared Modalities. To explore the underlying causes of MLLMs’ poor performance on thermal and infrared person ReID tasks, we conduct additional experiments on RGB and group ReID tasks, where the MLLMs perform relatively well. Specifically, all images are converted to grayscale to eliminate the influence of color information. As reported in Tab. 4, the results show a moderate decline in performance compared with the original setting. However, most MLLMs

Table 4. Results on grayscale RGB and group person ReID tasks. Rank@1, Rank@5, Rank@10, and mAP are delimited by slashes. The best and second-best results of Rank@1 and mAP are in **bold** and underlined, respectively.

Model	RGB	Group
Traditional Models:		
TransReID	0.24/0.42/0.50/0.33	0.16/0.28/0.34/0.23
Open-Source MLLMs:		
Qwen2.5-VL-3B	0.02/0.10/0.12/0.05	0.04/0.14/0.18/0.09
Qwen2.5-VL-7B	0.16/0.32/0.38/0.23	0.20/0.36/0.52/0.29
Qwen2.5-VL-32B	0.12/0.30/0.34/0.20	0.28/0.54/0.60/0.39
Qwen3-VL-2B	<u>0.28</u> /0.40/0.48/0.35	0.28/0.38/0.50/0.36
Qwen3-VL-4B	0.22/0.40/0.52/0.33	0.46/0.70/0.78/0.57
Qwen3-VL-8B	0.26/0.46/0.58/0.37	<u>0.56</u> /0.80/0.82/0.64
Qwen3-VL-32B	0.38 /0.46/0.52/0.42	0.66 /0.86/0.90/0.76
InternVL3.5-8B	0.00/0.02/0.02/0.01	0.02/0.02/0.06/0.04
InternVL3.5-38B	0.08/0.18/0.22/0.13	0.04/0.10/0.12/0.08

still maintain high performance. Notably, Qwen3-VL-32B achieves 0.66 in Rank@1 and 0.76 in mAP on the group ReID task. These findings suggest that the absence of color information is not the primary factor contributing to the poor performance of MLLMs on thermal and infrared person ReID tasks. Instead, the main limitation lies in the visual encoders of MLLMs, which have not been sufficiently trained on large-scale thermal and infrared datasets.

Chat-based Person ReID. Recently, the person ReID research community has witnessed a surge of interest in chat-based person ReID methods. Therefore, we also compare the performance of these approaches with that of MLLMs. The evaluation is conducted on the test set of the ChatPedes [3] dataset, where the chats are first transformed into descriptive sentences by Qwen3-VL-8B and are subsequently fed into the MLLMs for inference. It is worth noting that IRRA and DiaNA are trained on the training set of the ChatPedes dataset, while the MLLMs operate in a completely training-free manner. Despite this, the results in Tab. 5 show that Qwen3-VL-2B obtains 0.44 on Rank@1 and 0.41 on mAP, reaching competitive performance with

Table 5. Comparisons of IRRA, DiaNA, Qwen3-VL-2B, and Qwen3-VL-4B on chat-based person ReID task. The best and second-best results of Rank@1 and mAP are in **bold** and underlined, respectively

Models	IRRA [19]	DiaNA [3]	Qwen3-VL-2B [52]	Qwen3-VL-4B [52]
Rank@1/@5/@10/mAP	0.48/0.68/0.76/0.45	0.76/0.91/0.95/0.67	0.44/0.62/0.68/0.41	<u>0.52/0.69/0.77/0.49</u>

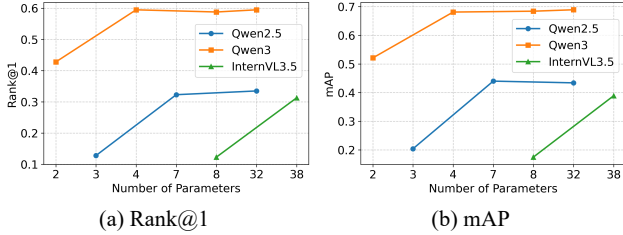


Figure 4. Scaling behavior of different model families on our VP-ReID. We report their averaged Rank@1 and mAP on eight tasks.

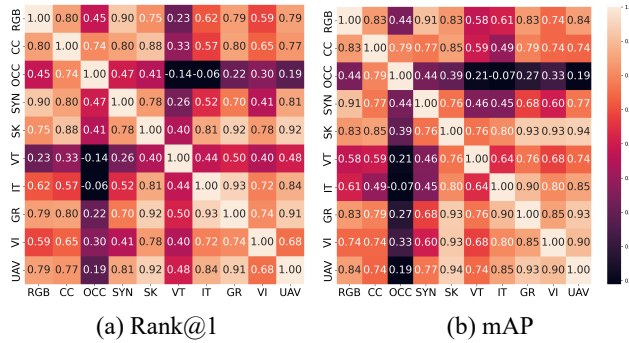


Figure 5. Correlation across different tasks in VP-ReID.

IRRA. Moreover, Qwen3-VL-4B achieves further gains, indicating a strong potential to approach state-of-the-art performance when trained on ChatPedes.

4.3. In-Depth Analyses

Scaling Behavior. To exemplify how MLLMs benefit from scaling laws on person ReID tasks, we averaged their Rank@1 and mAP on our VP-ReID (excluding thermal and infrared person ReID) and visualized the results in Fig. 4. The overall averaged performance adheres to the expected scaling trend, underscoring the potential of scaling MLLMs for improving person ReID capabilities. Nevertheless, we also notice that larger models within the same family do not always outperform their smaller counterparts, which may be caused by the substantial modality gap between these and RGB-based tasks. As shown in Tab. 3, Qwen3-VL-8B performs worse than Qwen3-VL-4B on cloth-changing and text person ReID tasks. A similar trend can be observed in the Qwen2.5-VL family, where Qwen2.5-VL-32B does not consistently surpass Qwen2.5-VL-7B.

Correlation Analysis. We present an analysis of the cor-

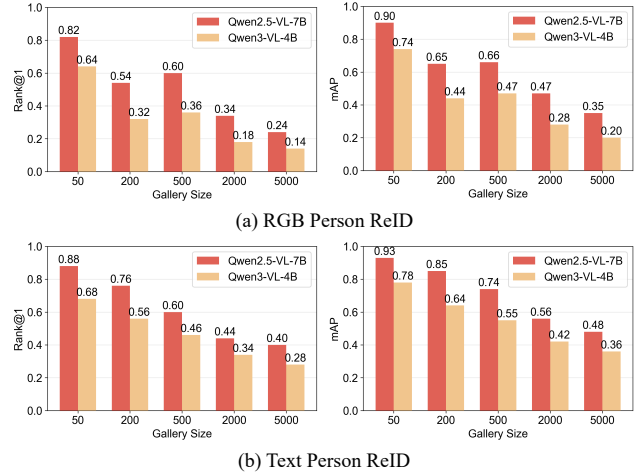


Figure 6. Impact of gallery size on the Rank@1 and mAP of Qwen2.5-VL-7B and Qwen3-VL-4B.

relation among different person ReID tasks. Specifically, we compute the Pearson correlation coefficient among all tasks in VP-ReID. The results are illustrated in Fig. 5. It can be observed that the RGB, cloth-changing, synthetic, sketch, group, and UAV person ReID tasks all correlate with one another. Interestingly, the MLLMs exhibit a strong performance correlation between sketch and other person ReID tasks, which may be attributed to substantial exposure to sketch-related data during their training process. In contrast, occluded, thermal, text, and infrared person ReID tasks correlate relatively weakly with all other tasks. That is because these tasks predominantly involve cross-modal scenarios or exhibit a substantial modality gap compared to the standard RGB person ReID task. These findings suggest that the future development of MLLM-based person ReID methods should prioritize addressing these disparate modalities rather than focusing on strongly correlated ones, thereby advancing the field toward a more comprehensive cross-modal understanding.

Inference Speed and Acceleration. The inference speed of MLLMs has long been a concern in person ReID. However, recent advancements have introduced various methods to optimize the inference speed of MLLMs. We deployed Qwen3-VL-2B and Qwen3-VL-4B using vLLM and evaluated their Rank@1, mAP, and per-query inference time on RGB, text, and group person ReID tasks. As illustrated in Tab. 6, both models achieve a substantial increase in infer-

Table 6. Comparisons of Rank@1, mAP, and per-query inference time of Qwen3-VL-2B and Qwen3-VL-4B on RGB, text, group person ReID tasks. The performance before and after deployment with vLLM are delimited by slashes.

Models	RGB			Text			Group		
	Rank@1	mAP	Time(s)	Rank@1	mAP	Time(s)	Rank@1	mAP	Time(s)
Qwen3-VL-2B [52]	0.34/0.34	0.43/0.44	37.6/4.88	0.48/0.44	0.58/0.56	59.1/6.44	0.58/0.58	0.65/0.65	27.3/3.48
Qwen3-VL-4B [52]	0.60/0.58	0.66/0.66	43.2/5.64	0.60/0.66	0.74/0.78	62.5/8.00	0.72/0.72	0.80/0.80	31.2/4.24

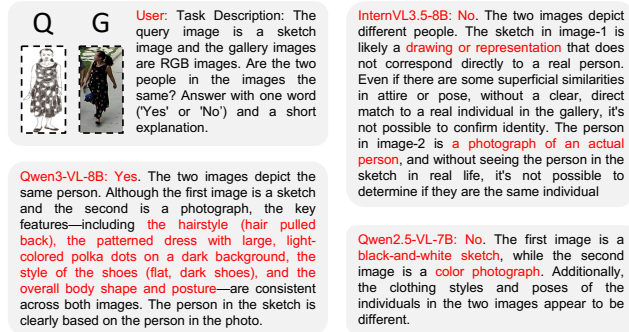


Figure 7. Qualitative comparisons of the sketch person ReID results from Qwen2.5-VL-7B, Qwen3-VL-8B, and InternVL3.5-8B.

ence speed without any loss of performance. In particular, their inference speed on the text person ReID task is 9.18× and 7.81× faster, respectively. It is worth noting that all of these results were obtained using MLLMs in 16-bit precision on a single NVIDIA RTX 4090 GPU. This implies that applying quantization techniques or hardware could further accelerate inference speeds.

Impact of Gallery Size. To investigate the impact of gallery size on the RGB and text person ReID tasks, we performed experiments by varying the gallery size from 50 to 5,000. The results can be found in Fig. 6. We first observe that Qwen2.5-VL-7B and Qwen3-VL-4B experience a sharp performance drop as the gallery size increases to 500. Beyond this point, although the performance continues to decline with larger gallery sizes, the rate of degradation becomes significantly slower. In addition, both models maintain relatively stable performance on the text person ReID task, highlighting the strong vision–language cross-modal understanding capabilities of MLLMs. Finally, Qwen3-VL-4B demonstrates greater robustness to variations in gallery size compared with Qwen2.5-VL-7B. When the gallery size reaches 5,000, Qwen3-VL-4B achieves 0.40 in Rank@1 and 0.48 in mAP on the text person ReID task, which is approximately half of its performance when the gallery size is 50.

Qualitative Comparisons. Compared with traditional person ReID models, MLLMs offer stronger interpretability, allowing for clearer insights into their reasoning processes. We modify the original prompt to generate brief explanations for the answers provided by MLLMs. The ex-

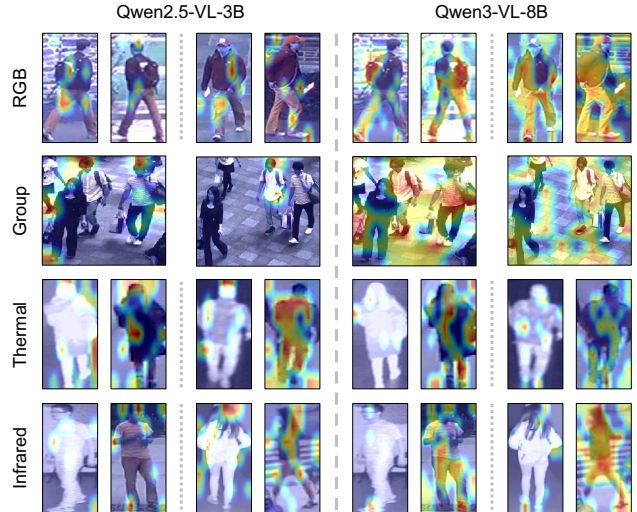


Figure 8. Attention maps of the RGB, group, thermal, and infrared person ReID results from Qwen2.5-VL-3B and Qwen3-VL-8B.

periments are conducted on the sketch person ReID task, which is widely adopted in forensic applications but remains highly challenging due to the unsatisfactory performance of most models. The results are presented in Fig. 7. Given a sketch image, Qwen3-VL-8B precisely captures fine-grained features such as hairstyle, dress patterns, shoe style, and overall body shape and posture. In contrast, Qwen2.5-VL-7B and InternVL3.5-8B primarily focus on modality differences and fail to extract high-level semantic information from these images, leading to incorrect results.

4.4. Visualizations

To provide an intuitive understanding and further validate the effectiveness of MLLMs in person ReID, we conduct a qualitative analysis in which the visualization of attention maps from the MLLM language decoder is shown in Fig. 8. Specifically, we present examples from group, thermal, and infrared person ReID, each with two query images and two gallery images (one for group ReID). The visualization results reveal that MLLMs are capable of effectively capturing high-level semantic information while simultaneously attending to fine-grained appearance details. For instance, Qwen3-VL-8B precisely identifies the key features that distinguish different individuals in the RGB person ReID task.

In the first example, the model primarily focuses on the carried bag. Furthermore, when the bag is occluded in the second example, its attention shifts toward the subject’s posture instead. In contrast, we observe that Qwen2.5-VL-3B fails to capture discriminative features between query and gallery images. This also explains the model’s poor performance in thermal and infrared person ReID tasks, where limited attention is concentrated on the relevant regions.

5. Conclusion

In this paper, we propose VP-ReID, a versatile person ReID benchmark specifically designed for MLLMs. The VP-ReID includes 257,310 multi-modal queries and gallery images, covering two evaluation schemes and ten different person ReID tasks. Extensive experiments demonstrate that MLLMs achieve impressive performance in various person ReID tasks. However, they also struggle with challenging thermal and infrared modalities, which require comprehensive cross-modal understanding capabilities and professional domain knowledge. Additionally, our findings reveal that some families of MLLMs adhere to the scaling law in person ReID tasks, exhibiting correlated performance when dealing with similar modalities. We hope these results can provide insights into the future improvements of MLLMs for effective and versatile person ReID.

Find Them All: Unveiling MLLMs for Versatile Person Re-identification

Supplementary Material

Table 7. Results of Qwen2.5-VL family on our real-world demonstration. The best and second-best results are in **bold** and underlined, respectively.

Models	Precision \uparrow	Recall \uparrow	F1 score \uparrow
Qwen2.5-VL-3B	0.640	0.300	0.408
Qwen2.5-VL-7B	<u>0.763</u>	<u>0.867</u>	<u>0.812</u>
Qwen2.5-VL-32B	0.757	0.893	0.819
Qwen2.5-VL-72B	0.787	0.800	0.793

A. Real-world Demonstration

Existing video-based person ReID datasets predominantly consist of pre-cropped pedestrian tracks, which exhibit considerable disparity from raw surveillance footage in real-world scenarios. To facilitate the real-world applications of MLLM-based person ReID methods, we propose a video-based person ReID dataset that maintains a similar data structure to MMReID-Bench. The detailed construction pipeline is illustrated in Fig. 9. We first collect source data from three real-world video datasets: Fitness-AQA [35], CAVIAR [10], and KTH Action [38]. Then, the collected data is captioned by GPT-4.1 in a structured format. Finally, question-answer pairs are generated by shuffling and matching the videos and captions.

As shown in Fig. 9, the inputs of our demonstration consist of a video clip and a textual description, which are widely used in forensic applications. We consider a scenario in which multiple witnesses provide different descriptions of a suspect at a crime scene. The police summarize the descriptions and search for the suspect across the surveillance footage using MLLMs. Ultimately, the MLLMs analyze the videos and output the identified target.

Given their competitive performance and open-source availability, we adopt the Qwen2.5-VL family for our experiments. The results are presented in Tab. 7. It can be observed that even Qwen2.5-VL-7B achieves a notable F1 score of 0.812. We assume that this can be attributed to the fine-grained descriptions generated by GPT-4.1, which may not be available in real-world scenarios. However, as a case progresses, increasing amounts of evidence and witness testimonies will gradually accumulate. Consequently, the descriptions of the suspect will become more detailed and will closely resemble the conditions in our experimental setup. Therefore, the results of our experiments hold substantial practical relevance for real-world forensic applications.

Table 8. Detailed Prompts for the QGM.

Prompt for the Image-based (Exclude Group) Person ReID:

You are a person re-identification assistant. Are the two people in the images the same? Answer strictly with only one word: ‘Yes’ or ‘No’.

Prompt for the Group ReID:

You are a person re-identification assistant. Are the two group of people in the images the same? Answer strictly with only one word: ‘Yes’ or ‘No’.

Prompt for the Text Person ReID:

You are a person re-identification assistant. Your task is to carefully analyze the descriptions of the person in the following text and determine whether the image shows the same person. \<text> \strictly with only one word: ‘Yes’ or ‘No’.

B. Detailed Prompts for the QGM

In this section, we provide the prompts used for the QGM, as detailed in Tab. 8. The placeholders for text and images need to be adjusted accordingly for different models.

C. Detailed Prompts for the MCQ

In this section, we provide the prompts used for the MCQ, as detailed in Tab. 9. The placeholders for text and images need to be adjusted accordingly for different models.

D. More Inference Examples

We show the results of Qwen3-VL-8B on 10 person ReID tasks in Fig. 10. Note that we modify the original prompt to generate a short explanation.

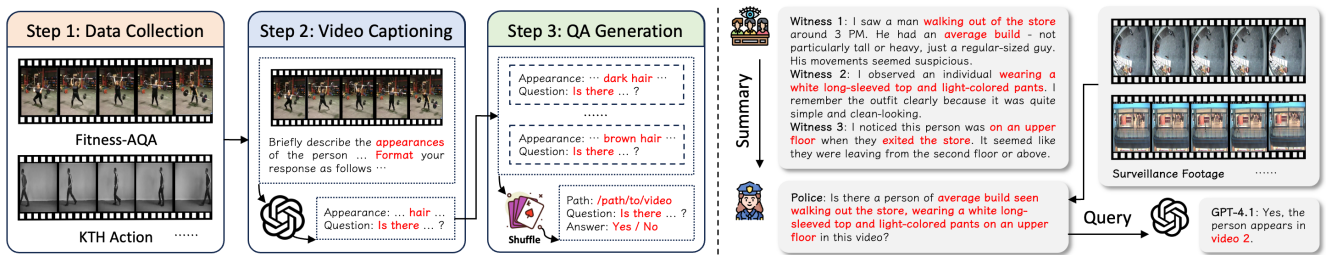


Figure 9. Overview of the real-world demonstration. Left: the construction pipeline of the test set used in the real-world demonstration. Right: a simulation case illustrating forensic applications.

Table 9. Detailed Prompts for the MCQ.

Prompt for the Cloth-changing Person ReID:

Query Image: < image 1 > \n Gallery Images: < image 1 > < image 2 > < image 3 > < image 4 > \n Task Description: The people in the query image and gallery images wear different clothes. Your task is to carefully analyze the appearance, and pose of the person in the query image and determine which gallery image shows the same person. Please answer with the letter of the correct option directly (A, B, C, or D) and no other text.

Prompt for the RGB Person ReID:

Query Image: < image 1 > \n Gallery Images: < image 1 > < image 2 > < image 3 > < image 4 > \n Task Description: The query and gallery images are all RGB images. Your task is to carefully analyze the appearance, clothing, and pose of the person in the query image and determine which gallery image shows the same person. Please answer with the letter of the correct option directly (A, B, C, or D) and no other text.

Prompt for the Occluded Person ReID:

Query Image: < image 1 > \n Gallery Images: < image 1 > < image 2 > < image 3 > < image 4 > \n Task Description: The query image is a thermal image and the gallery images are RGB images. Your task is to carefully analyze the body structure, contour features, thermal pattern, gait/motion pattern, background information, and other details of the person in the query image and determine which gallery image shows the same person. Please answer with the letter of the correct option directly (A, B, C, or D) and no other text.

Prompt for the Synthetic Person ReID:

Query Image: < image 1 > \n Gallery Images: < image 1 > < image 2 > < image 3 > < image 4 > \n Task Description: The query and gallery images are all synthetic. Your task is to carefully analyze the appearance, clothing, and pose of the person in the query image and determine which gallery image shows the same person. Please answer with the letter of the correct option directly (A, B, C, or D) and no other text.

Prompt for the Sketch Person ReID:

Query Image: < image 1 > \n Gallery Images: < image 1 > < image 2 > < image 3 > < image 4 > \n Task Description: The query image is a sketch image and the gallery images are RGB images. Your task is to carefully analyze the appearance, clothing, and pose of the person in the query image and determine which gallery image shows the same person. Please answer with the letter of the correct option directly (A, B, C, or D) and no other text.

Prompt for the Thermal ReID:

Query Image: < image 1 > \n Gallery Images: < image 1 > < image 2 > < image 3 > < image 4 > \n Task Description: The query image is a thermal image and the gallery images are RGB images. Your task is to carefully analyze the body structure, contour features, thermal pattern, gait/motion pattern, background information, and other details of the person in the query image and determine which gallery image shows the same person. Please answer with the letter of the correct option directly (A, B, C, or D) and no other text.

Prompt for the Text Person ReID:

Query Image: < text 1 > \n Gallery Images: < image 1 > < image 2 > < image 3 > < image 4 > \n Task Description: The query text contains 2 textual descriptions about the attributes of the target person. Your task is to carefully analyze the descriptions of the person in the query text and determine which gallery image shows the same person. Please answer with the letter of the correct option directly (A, B, C, or D) and no other text.

Prompt for the Group ReID:

Query Image: < image 1 > \n Gallery Images: < image 1 > < image 2 > < image 3 > < image 4 > \n Task Description: The query and gallery images are all RGB images. Your task is to carefully analyze the relative position, motion pattern, structure topology, interaction features, individual appearance, size, and density of the people in the query image and determine which gallery image shows the same people. Please answer with the letter of the correct option directly (A, B, C, or D) and no other text.

Prompt for the Infrared ReID:

Query Image: < image 1 > \n Gallery Images: < image 1 > < image 2 > < image 3 > < image 4 > \n Task Description: The query image is an infrared image and the gallery images are RGB images. Your task is to carefully analyze the body structure, contour features, thermal pattern, gait/motion pattern, background information, and other details of the person in the query image and determine which gallery image shows the same person. Please answer with the letter of the correct option directly (A, B, C, or D) and no other text.

Prompt for the UAV Person ReID:

Query Image: < image 1 > \n Gallery Images: < image 1 > < image 2 > < image 3 > < image 4 > \n Task Description: The query and gallery images are all UAV images. Your task is to carefully analyze the appearance, body structure, contour features, gait/motion pattern, background information, and other details of the person in the query image and determine which gallery image shows the same person. Please answer with the letter of the correct option directly (A, B, C, or D) and no other text.

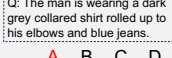
<p>Q A B C D</p>  <p>Cloth-changing</p>	<p>The people in the query image and gallery images wear different clothes. Your task is to carefully analyze the appearance, and pose of the person in the query image and determine which gallery image shows the same person. Select the correct answer in the following options: A <image 2>, B <image 3>, C <image 4>, D <image 5>. Please answer with the letter of the correct option (A, B, C, or D) and a short explanation.</p> <p>D. The person in the query image is wearing a dark uniform with a white hard hat and carrying a box. Image 5 shows the same person from a slightly different angle, also wearing the same uniform and hard hat and carrying the same box. The other images show people in completely different attire (a cyclist, a man in a purple shirt, a woman in a blue blazer).</p>
<p>Q A B C D</p>  <p>RGB</p>	<p>The query and gallery images are all RGB images. Your task is to carefully analyze the appearance, clothing, and pose of the person in the query image and determine which gallery image shows the same person. Select the correct answer in the following options: A <image 2>, B <image 3>, C <image 4>, D <image 5>. Please answer with the letter of the correct option (A, B, C, or D) and a short explanation.</p> <p>C. The person in the query image is a man with short brown hair, wearing a black jacket, blue jeans, and blue sneakers. He is carrying a blue bag in his left hand and has a backpack on. Image 4 shows the same person with the identical clothing, hairstyle, and pose, walking while carrying the blue bag. The other images show different individuals: Image 2 shows a person in a hooded jacket, Image 3 shows a man with a cap and different jacket style, and Image 5 shows a person in a dark hoodie and dark pants.</p>
<p>Q A B C D</p>  <p>Occluded</p>	<p>The query image is occluded by some objects and the gallery images are not occluded. Your task is to carefully analyze the appearance, clothing, and pose of the person in the query image and determine which gallery image shows the same person. Select the correct answer in the following options: A <image 2>, B <image 3>, C <image 4>, D <image 5>. Please answer with the letter of the correct option (A, B, C, or D) and a short explanation.</p> <p>D. The person in the query image is wearing a grey hoodie, blue jeans, and white sneakers, and is carrying a black backpack. They are also smiling and appear to be in motion. Gallery image D shows the same person in the same outfit (grey hoodie, blue jeans, white sneakers, black backpack) and in a similar pose, walking and smiling. The other gallery images show different people with different clothing and appearances.</p>
<p>Q A B C D</p>  <p>Synthetic</p>	<p>The query and gallery images are all synthetic. Your task is to carefully analyze the appearance, clothing, and pose of the person in the query image and determine which gallery image shows the same person. Select the correct answer in the following options: A <image 2>, B <image 3>, C <image 4>, D <image 5>. Please answer with the letter of the correct option (A, B, C, or D) and a short explanation.</p> <p>C. The person in the query image (image 1) is a woman with blonde hair, viewed from the back, wearing a light blue, sleeveless, A-line dress and black heeled shoes. Image 4 shows the same person from a side-back angle, wearing the identical light blue dress and black shoes. The other images show different individuals with different hair colors, clothing, and poses.</p>
<p>Q A B C D</p>  <p>Sketch</p>	<p>The query image is a sketch image and the gallery images are RGB images. Your task is to carefully analyze the appearance, clothing, and pose of the person in the query image and determine which gallery image shows the same person. Select the correct answer in the following options: A <image 2>, B <image 3>, C <image 4>, D <image 5>. Please answer with the letter of the correct option (A, B, C, or D) and a short explanation.</p> <p>C. The person in the query sketch is wearing a t-shirt with an Adidas logo and is carrying a backpack. Image 4 shows a boy wearing a blue Adidas t-shirt and carrying a backpack, matching the key identifying features. The other gallery images show different individuals with different clothing and accessories.</p>
<p>Q A B C D</p>  <p>Thermal</p>	<p>The query image is a thermal image and the gallery images are RGB images. Your task is to carefully analyze the body structure, contour features, thermal pattern, gait/motion pattern, background information, and other details of the person in the query image and determine which gallery image shows the same person. Select the correct answer in the following options: A <image 2>, B <image 3>, C <image 4>, D <image 5>. Please answer with the letter of the correct option (A, B, C, or D) and a short explanation.</p> <p>B. The query image is a thermal image showing a person with a very bright, uniform thermal signature, indicating a high body temperature relative to the environment. The figure is in a walking posture, with a slightly bent posture and arms possibly crossed or held near the chest. The most distinguishing feature is the very high thermal contrast, which makes the person appear as a bright white silhouette against a darker background. Looking at the gallery images: Image A: Shows a person from behind wearing a dark jacket with a red collar and dark pants. The thermal signature is not visible, and the person is not bright white. Image B: Shows a person from the front, wearing a dark jacket and dark pants, holding an object. The person's thermal signature is not visible, and the person is not bright white. Image C: Shows a person from the front, wearing a dark jacket and dark pants, holding an object. The person's thermal signature is not visible, and the person is not bright white. Image D: Shows a person from behind, wearing a dark jacket and dark pants. The thermal signature is not visible, and the person is not bright white. None of the gallery images show a person with the same thermal signature as the query image. However, the query image is extremely blurry and low-resolution, and the person's posture is not clearly defined. The most similar posture among the gallery images is Image B, which shows a person in a walking posture with arms held in front, which is somewhat similar to the posture in the query image. Therefore, despite the lack of thermal signature, Image B is the most likely match based on posture and general appearance. Note: This is a difficult match because the thermal signature in the query image is not present in any of the gallery images, making it impossible to match based on thermal pattern. The match is based on posture and general silhouette.</p>
<p>Q: The man is wearing a dark grey collared shirt rolled up to his elbows and blue jeans.</p> <p>A B C D</p>  <p>Text</p>	<p>The query text contains 2 textual descriptions about the attributes of the target person. Your task is to carefully analyze the descriptions of the person in the query text and determine which gallery image shows the same person. Select the correct answer in the following options: A <image 1>, B <image 2>, C <image 3>, D <image 4>. Please answer with the letter of the correct option DIRECTLY (A, B, C, or D) and no other text.</p> <p>A. The query text describes a man wearing a dark grey collared shirt rolled up to his elbows and blue jeans. Image 1 shows a man matching this description exactly: a dark grey collared shirt with sleeves rolled up, and blue jeans. The other images show different people in different clothing.</p>
<p>Q A B C D</p>  <p>Group</p>	<p>The query and gallery images are all RGB images. Your task is to carefully analyze the relative position, motion pattern, structure topology, interaction features, individual appearance, size, and density of the people in the query image and determine which gallery image shows the same people. Select the correct answer in the following options: A <image 2>, B <image 3>, C <image 4>, D <image 5>. Please answer with the letter of the correct option (A, B, C, or D) and a short explanation.</p> <p>D. The query image (Image 1) features two men walking on a paved sidewalk. The man in the foreground is wearing a white short-sleeved shirt and light-colored pants. The man behind him is wearing a light-colored, possibly white, shirt and dark pants, carrying a dark bag over his shoulder. In Image 5, the same two men are visible in a nearly identical pose and relative position, walking in the same direction. The man in the foreground is wearing the same white shirt and light pants, and the man behind him is wearing a similar light shirt and dark pants, also carrying a dark bag. The other gallery images show different groups of people and do not match the individuals in the query image.</p>
<p>Q A B C D</p>  <p>Infrared</p>	<p>The query image is an infrared image and the gallery images are RGB images. Your task is to carefully analyze the body structure, contour features, thermal pattern, gait/motion pattern, background information, and other details of the person in the query image and determine which gallery image shows the same person. Select the correct answer in the following options: A <image 2>, B <image 3>, C <image 4>, D <image 5>. Please answer with the letter of the correct option (A, B, C, or D) and a short explanation.</p> <p>D. The person in the query image (image 1) is wearing a dark t-shirt and light-colored shorts, and is standing with their body slightly turned. Comparing this to the gallery images, image 5 shows a person wearing a similar dark t-shirt (gray with a red graphic) and light-colored shorts (khaki or beige). The body posture and overall silhouette are also consistent. The other gallery images show different clothing (e.g., backpacks, different shirt colors, different pants) and different poses or settings, making them unlikely to be the same person.</p>
<p>Q A B C D</p>  <p>UAV</p>	<p>The query and gallery images are all UAV images. Your task is to carefully analyze the appearance, body structure, contour features, gait/motion pattern, background information, and other details of the person in the query image and determine which gallery image shows the same person. Select the correct answer in the following options: A <image 2>, B <image 3>, C <image 4>, D <image 5>. Please answer with the letter of the correct option (A, B, C, or D) and a short explanation.</p> <p>C. The person in the query image (Image 1) is wearing a red cap and a black polo shirt. In Image 4, the person is also wearing a black polo shirt and a red cap, and they are standing in a similar pose with their hands clasped. Although the lighting and background differ, the combination of the red cap, black polo shirt, and body posture strongly indicates that it is the same person. The other gallery images show different clothing and poses, making them less likely matches.</p>

Figure 10. More inference examples from Qwen3-VL-8B in the MCQ. We highlight the correct answers in red.

References

- [1] Jean-Baptiste Alayrac, Jeff Donahue, Pauline Luc, Antoine Miech, Iain Barr, Yana Hasson, Karel Lenc, Arthur Mensch, Katherine Millican, Malcolm Reynolds, et al. Flamingo: a visual language model for few-shot learning. *Advances in neural information processing systems*, 35:23716–23736, 2022. 2
- [2] Shuai Bai, Keqin Chen, Xuejing Liu, Jialin Wang, Wenbin Ge, Sibao Song, Kai Dang, Peng Wang, Shijie Wang, Jun Tang, et al. Qwen2. 5-vl technical report. *arXiv preprint arXiv:2502.13923*, 2025. 4, 5
- [3] Yang Bai, Yucheng Ji, Min Cao, Jinqiao Wang, and Mang Ye. Chat-based person retrieval via dialogue-refined cross-modal alignment. In *Proceedings of the Computer Vision and Pattern Recognition Conference*, pages 3952–3962, 2025. 6, 7
- [4] Zechen Bai, Zhigang Wang, Jian Wang, Di Hu, and Errui Ding. Unsupervised multi-source domain adaptation for person re-identification. In *Proceedings of the IEEE/CVF conference on computer vision and pattern recognition*, pages 12914–12923, 2021. 3
- [5] Liping Bao, Longhui Wei, Xiaoyu Qiu, Wengang Zhou, Houqiang Li, and Qi Tian. Learning transferable pedestrian representation from multimodal information supervision. *arXiv preprint arXiv:2304.05554*, 2023. 2
- [6] Hongxu Chen, Quan Zhang, Jian-Huang Lai, and Xiaohua Xie. Unsupervised group re-identification via adaptive clustering-driven progressive learning. In *Proceedings of the AAAI Conference on Artificial Intelligence*, pages 1054–1062, 2024. 2
- [7] Zhe Chen, Weiyun Wang, Yue Cao, Yangzhou Liu, Zhangwei Gao, Erfei Cui, Jinguo Zhu, Shenglong Ye, Hao Tian, Zhaoyang Liu, et al. Expanding performance boundaries of open-source multimodal models with model, data, and test-time scaling. *arXiv preprint arXiv:2412.05271*, 2024. 4
- [8] Zijian Chen, Yuan Tian, Yuze Sun, Wei Sun, Zicheng Zhang, Weisi Lin, Guangtao Zhai, and Wenjun Zhang. Just noticeable difference for large multimodal models. *arXiv preprint arXiv:2507.00490*, 2025. 2
- [9] De Cheng, Xiaojian Huang, Nannan Wang, Lingfeng He, Zhihui Li, and Xinbo Gao. Unsupervised visible-infrared person reid by collaborative learning with neighbor-guided label refinement. In *Proceedings of the 31st ACM international conference on multimedia*, pages 7085–7093, 2023. 3
- [10] Dong Seon Cheng, Marco Cristani, Michele Stoppa, Loris Bazzani, Vittorio Murino, et al. Custom pictorial structures for re-identification. In *Bmvc*, page 6, 2011. 1
- [11] Wenbo Dai, Lijing Lu, and Zhihang Li. Diffusion-based synthetic data generation for visible-infrared person re-identification. In *Proceedings of the AAAI Conference on Artificial Intelligence*, pages 11185–11193, 2025. 2
- [12] Yongxing Dai, Jun Liu, Yifan Sun, Zekun Tong, Chi Zhang, and Ling-Yu Duan. Idm: An intermediate domain module for domain adaptive person re-id. In *Proceedings of the IEEE/CVF international conference on computer vision*, pages 11864–11874, 2021. 3
- [13] Zefeng Ding, Changxing Ding, Zhiyin Shao, and Dacheng Tao. Semantically self-aligned network for text-to-image part-aware person re-identification. *arXiv preprint arXiv:2107.12666*, 2021. 6
- [14] Alexey Dosovitskiy, Lucas Beyer, Alexander Kolesnikov, Dirk Weissenborn, Xiaohua Zhai, Thomas Unterthiner, Mostafa Dehghani, Matthias Minderer, Georg Heigold, Sylvain Gelly, et al. An image is worth 16x16 words: Transformers for image recognition at scale. *arXiv preprint arXiv:2010.11929*, 2020. 3
- [15] Shuting He, Hao Luo, Pichao Wang, Fan Wang, Hao Li, and Wei Jiang. Transreid: Transformer-based object re-identification. In *Proceedings of the IEEE/CVF international conference on computer vision*, pages 15013–15022, 2021. 4, 5
- [16] Weizhen He, Yiheng Deng, Shixiang Tang, Qihao Chen, Qingsong Xie, Yizhou Wang, Lei Bai, Feng Zhu, Rui Zhao, Wanli Ouyang, et al. Instruct-reid: A multi-purpose person re-identification task with instructions. In *Proceedings of the IEEE/CVF Conference on Computer Vision and Pattern Recognition*, pages 17521–17531, 2024. 2, 3
- [17] Zhangyi Hu, Bin Yang, and Mang Ye. Empowering visible-infrared person re-identification with large foundation models. *Advances in Neural Information Processing Systems*, 37: 117363–117387, 2024. 2, 3
- [18] Wenke Huang, Yuxia Liu, Mang Ye, Jun Chen, and Bo Du. Federated learning with long-tailed data via representation unification and classifier rectification. *IEEE Transactions on Information Forensics and Security*, 19:5738–5750, 2024. 2
- [19] Ding Jiang and Mang Ye. Cross-modal implicit relation reasoning and aligning for text-to-image person retrieval. In *Proceedings of the IEEE/CVF conference on computer vision and pattern recognition*, pages 2787–2797, 2023. 5, 7
- [20] Jiayu Jiang, Changxing Ding, Wentao Tan, Junhong Wang, Jin Tao, and Xiangmin Xu. Modeling thousands of human annotators for generalizable text-to-image person re-identification. In *Proceedings of the Computer Vision and Pattern Recognition Conference*, pages 9220–9230, 2025. 2, 3
- [21] Yan Jiang, Xu Cheng, Hao Yu, Xingyu Liu, Haoyu Chen, and Guoying Zhao. Domain shifting: A generalized solution for heterogeneous cross-modality person re-identification. In *European Conference on Computer Vision*, pages 289–306. Springer, 2024. 2
- [22] He Li, Mang Ye, and Bo Du. Weperson: Learning a generalized re-identification model from all-weather virtual data. In *Proceedings of the 29th ACM international conference on multimedia*, pages 3115–3123, 2021. 3
- [23] Shuang Li, Tong Xiao, Hongsheng Li, Bolei Zhou, Dayu Yue, and Xiaogang Wang. Person search with natural language description. In *Proceedings of the IEEE conference on computer vision and pattern recognition*, pages 1970–1979, 2017. 4
- [24] Tianjiao Li, Jun Liu, Wei Zhang, Yun Ni, Wenqian Wang, and Zhiheng Li. Uav-human: A large benchmark for human behavior understanding with unmanned aerial vehicles. In *Proceedings of the IEEE/CVF conference on computer vision and pattern recognition*, pages 16266–16275, 2021. 4

- [25] Wen Li, Cheng Zou, Meng Wang, Furong Xu, Jianan Zhao, Ruobing Zheng, Yuan Cheng, and Wei Chu. Dc-former: Diverse and compact transformer for person re-identification. In *Proceedings of the AAAI Conference on Artificial Intelligence*, pages 1415–1423, 2023. 3
- [26] Yubo Li, De Cheng, Chaowei Fang, Changzhe Jiao, Nan-nan Wang, and Xinbo Gao. Disentangling identity features from interference factors for cloth-changing person re-identification. In *Proceedings of the 32nd ACM International Conference on Multimedia*, pages 2252–2261, 2024. 2
- [27] Weiyao Lin, Yuxi Li, Hao Xiao, John See, Junni Zou, Hongkai Xiong, Jingdong Wang, and Tao Mei. Group re-identification with multigrained matching and integration. *IEEE transactions on cybernetics*, 51(3):1478–1492, 2019. 4
- [28] Yongguo Ling, Zhun Zhong, Zhiming Luo, Fengxiang Yang, Donglin Cao, Yaojin Lin, Shaozi Li, and Nicu Sebe. Cross-modality earth mover’s distance for visible thermal person re-identification. In *Proceedings of the AAAI conference on artificial intelligence*, pages 1631–1639, 2023. 2
- [29] Haotian Liu, Chunyuan Li, Qingyang Wu, and Yong Jae Lee. Visual instruction tuning. *Advances in neural information processing systems*, 36:34892–34916, 2023. 2
- [30] Dat Tien Nguyen, Hyung Gil Hong, Ki Wan Kim, and Kang Ryoung Park. Person recognition system based on a combination of body images from visible light and thermal cameras. *Sensors*, 17(3):605, 2017. 4
- [31] Hao Ni, Jingkuan Song, Xiaopeng Luo, Feng Zheng, Wen Li, and Heng Tao Shen. Meta distribution alignment for generalizable person re-identification. In *Proceedings of the IEEE/CVF conference on computer vision and pattern recognition*, pages 2487–2496, 2022. 3
- [32] OpenAI. Hello gpt-4o. <https://openai.com/index/hello-gpt-4o>, 2024. Accessed: 2025-08-01. 4, 5
- [33] OpenAI. Gpt-4-1. <https://openai.com/index/gpt-4-1>, 2025. Accessed: 2025-08-01. 4, 5
- [34] Lu Pang, Yaowei Wang, Yi-Zhe Song, Tiejun Huang, and Yonghong Tian. Cross-domain adversarial feature learning for sketch re-identification. In *Proceedings of the 26th ACM international conference on Multimedia*, pages 609–617, 2018. 4
- [35] Paritosh Parmar, Amol Gharat, and Helge Rhodin. Domain knowledge-informed self-supervised representations for workout form assessment. In *European Conference on Computer Vision*, pages 105–123. Springer, 2022. 1
- [36] Sundar Pichai, Demis Hassabis, and Koray Kavukcuoglu. Introducing gemini 2.0: our new ai model for the agentic era. <https://blog.google/technology/google-deepmind/google-gemini-ai-update-december-2024/>, 2024. Accessed: 2025-07-05. 4, 5
- [37] Haocong Rao, Cyril Leung, and Chunyan Miao. Hierarchical skeleton meta-prototype contrastive learning with hard skeleton mining for unsupervised person re-identification. *International Journal of Computer Vision*, 132(1):238–260, 2024. 3
- [38] Peter M Roth, Thomas Mauthner, Inayatullah Khan, and Horst Bischof. Efficient human action recognition by cascaded linear classification. In *2009 IEEE 12th International Conference on Computer Vision Workshops, ICCV Workshops*, pages 546–553. IEEE, 2009. 1
- [39] Xiaoxiao Sun and Liang Zheng. Dissecting person re-identification from the viewpoint of viewpoint. In *Proceedings of the IEEE/CVF conference on computer vision and pattern recognition*, pages 608–617, 2019. 4
- [40] Lei Tan, Jiaer Xia, Wenfeng Liu, Pingyang Dai, Yongjian Wu, and Liujuan Cao. Occluded person re-identification via saliency-guided patch transfer. In *Proceedings of the AAAI conference on artificial intelligence*, pages 5070–5078, 2024. 2
- [41] Wentan Tan, Changxing Ding, Jiayu Jiang, Fei Wang, Yibing Zhan, and Dapeng Tao. Harnessing the power of mllms for transferable text-to-image person reid. In *Proceedings of the IEEE/CVF Conference on Computer Vision and Pattern Recognition*, pages 17127–17137, 2024. 3
- [42] Gemini Team, Petko Georgiev, Ving Ian Lei, Ryan Burnell, Libin Bai, Anmol Gulati, Garrett Tanzer, Damien Vincent, Zhufeng Pan, Shibo Wang, et al. Gemini 1.5: Unlocking multimodal understanding across millions of tokens of context. *arXiv preprint arXiv:2403.05530*, 2024. 4, 5
- [43] Weiyun Wang, Zhangwei Gao, Lixin Gu, Hengjun Pu, Long Cui, Xingguang Wei, Zhaoyang Liu, Linglin Jing, Shenglong Ye, Jie Shao, et al. Internvl3.5: Advancing open-source multimodal models in versatility, reasoning, and efficiency. *arXiv preprint arXiv:2508.18265*, 2025. 4, 5
- [44] Yuhao Wang, Yongfeng Lv, Pingping Zhang, and Huchuan Lu. Idea: Inverted text with cooperative deformable aggregation for multi-modal object re-identification. In *Proceedings of the Computer Vision and Pattern Recognition Conference*, pages 29701–29710, 2025. 2, 3
- [45] Ancong Wu, Wei-Shi Zheng, Hong-Xing Yu, Shaogang Gong, and Jianhuang Lai. Rgb-infrared cross-modality person re-identification. In *Proceedings of the IEEE international conference on computer vision*, pages 5380–5389, 2017. 4
- [46] Haoning Wu, Zicheng Zhang, Erli Zhang, Chaofeng Chen, Liang Liao, Annan Wang, Chunyi Li, Wenxiu Sun, Qiong Yan, Guangtao Zhai, et al. Q-bench: A benchmark for general-purpose foundation models on low-level vision. *arXiv preprint arXiv:2309.14181*, 2023. 4
- [47] Jinlin Wu, Lingxiao He, Wu Liu, Yang Yang, Zhen Lei, Tao Mei, and Stan Z Li. Cavit: Contextual alignment vision transformer for video object re-identification. In *European Conference on Computer Vision*, pages 549–566. Springer, 2022. 3
- [48] Pengfei Wu, Le Wang, Sanping Zhou, Gang Hua, and Changyin Sun. Temporal correlation vision transformer for video person re-identification. In *Proceedings of the AAAI Conference on Artificial Intelligence*, pages 6083–6091, 2024. 3
- [49] xAI. Grok-2. <https://x.ai/news/grok-2>, 2024. Accessed: 2025-08-01. 4, 5
- [50] xAI. Grok-4. <https://x.ai/news/grok-4>, 2025. Accessed: 2025-08-01. 4, 5

- [51] Peng Xu and Xiatian Zhu. Deepchange: A long-term person re-identification benchmark with clothes change. In *Proceedings of the IEEE/CVF International Conference on Computer Vision*, pages 11196–11205, 2023. 4
- [52] An Yang, Anfeng Li, Baosong Yang, Beichen Zhang, Binyuan Hui, Bo Zheng, Bowen Yu, Chang Gao, Chengen Huang, Chenxu Lv, et al. Qwen3 technical report. *arXiv preprint arXiv:2505.09388*, 2025. 4, 5, 7, 8
- [53] Bin Yang, Jun Chen, and Mang Ye. Towards grand unified representation learning for unsupervised visible-infrared person re-identification. In *Proceedings of the IEEE/CVF International Conference on Computer Vision*, pages 11069–11079, 2023. 3
- [54] Mang Ye, Jianbing Shen, Gaojie Lin, Tao Xiang, Ling Shao, and Steven CH Hoi. Deep learning for person re-identification: A survey and outlook. *IEEE transactions on pattern analysis and machine intelligence*, 44(6):2872–2893, 2021. 2
- [55] Mang Ye, Zesen Wu, Cuiqun Chen, and Bo Du. Channel augmentation for visible-infrared re-identification. *IEEE Transactions on Pattern Analysis and Machine Intelligence*, 46(4):2299–2315, 2023. 2
- [56] Mang Ye, Shuoyi Chen, Chenyue Li, Wei-Shi Zheng, David Crandall, and Bo Du. Transformer for object re-identification: A survey. *International Journal of Computer Vision*, pages 1–31, 2024. 3
- [57] Yajing Zhai, Yawen Zeng, Zhiyong Huang, Zheng Qin, Xin Jin, and Da Cao. Multi-prompts learning with cross-modal alignment for attribute-based person re-identification. In *Proceedings of the AAAI Conference on Artificial Intelligence*, pages 6979–6987, 2024. 2, 3
- [58] Qiang Zhang, Changzhou Lai, Jianan Liu, Nianchang Huang, and Jungong Han. Fmcnet: Feature-level modality compensation for visible-infrared person re-identification. In *Proceedings of the IEEE/CVF conference on computer vision and pattern recognition*, pages 7349–7358, 2022. 2
- [59] Quan Zhang, Lei Wang, Vishal M Patel, Xiaohua Xie, and Jianhaung Lai. View-decoupled transformer for person re-identification under aerial-ground camera network. In *Proceedings of the IEEE/CVF Conference on Computer Vision and Pattern Recognition*, pages 22000–22009, 2024. 2
- [60] Liang Zheng, Liyue Shen, Lu Tian, Shengjin Wang, Jingdong Wang, and Qi Tian. Scalable person re-identification: A benchmark. In *Proceedings of the IEEE international conference on computer vision*, pages 1116–1124, 2015. 6
- [61] Zhedong Zheng, Liang Zheng, and Yi Yang. Unlabeled samples generated by gan improve the person re-identification baseline in vitro. In *Proceedings of the IEEE international conference on computer vision*, pages 3754–3762, 2017. 4
- [62] Haowei Zhu, Wenjing Ke, Dong Li, Ji Liu, Lu Tian, and Yi Shan. Dual cross-attention learning for fine-grained visual categorization and object re-identification. In *Proceedings of the IEEE/CVF conference on computer vision and pattern recognition*, pages 4692–4702, 2022. 3
- [63] Jinguo Zhu, Weiyun Wang, Zhe Chen, Zhaoyang Liu, Shenglong Ye, Lixin Gu, Hao Tian, Yuchen Duan, Weijie Su, Jie Shao, et al. Internv13: Exploring advanced training and test-time recipes for open-source multimodal models. *arXiv preprint arXiv:2504.10479*, 2025. 4
- [64] Jiakuan Zhuo, Zeyu Chen, Jianhuang Lai, and Guangcong Wang. Occluded person re-identification. In *2018 IEEE international conference on multimedia and expo (ICME)*, pages 1–6. IEEE, 2018. 4